

# Spontaneous Electric Polarization in Graphene Polytypes

Simon Salleh Atri, Wei Cao, Bar Alon, Nirmal Roy, Maayan Vizner Stern, Vladimir Falko, Moshe Goldstein, Leeor Kronik, Michael Urbakh, Oded Hod, and Moshe Ben Shalom\*

Spontaneous electric polarization is recently observed in multilayered van der Waals stacked materials, arising from a symmetry breaking in a unit cell with two or more constituent species, or non-centrosymmetric intra-layer atom displacement in single-atom-species materials. Here, it is shown that even elemental crystals, consisting of one type of atom and composed of non-polar and centrosymmetric layers, exhibit electric polarization if arranged in an appropriate three-dimensional architecture. This concept is demonstrated here for mixed-stacking tetra-layer polytypes of non-polar graphene sheets. Surprisingly, it is found that the room temperature out-of-plane electric polarization increases with external electrostatic hole doping, rather than decreases with it owing to screening. Using first-principles calculations, as well as a self-consistent tight-binding model, the emergence of polarization is explained in terms of inter-layer charge rearrangement and the doping dependence in terms of gating-induced inter-layer charge transfer. This newly discovered intrinsic polarization may therefore offer new venues for designing the electronic response of graphene-based polytypes to external fields.

## 1. Introduction

In crystalline van der Waals (vdW) multilayers, one can distinguish between crystal polytypes, i.e., polymorphs with structures that differ only along the out-of-plane direction.<sup>[1]</sup> In a two-dimensional (2D) vdW polytype, each successive layer is identical, but can stack in different metastable configurations that modify overall crystal properties,<sup>[2]</sup> notably spontaneous electric polarization.<sup>[3–6]</sup> For example, parallel stacking of diatomic hexagonal bilayers has been recently predicted and shown to result in permanent out-of-plane polarization,  $P_z$ , which is absent in the natural antiparallel stacking configuration.<sup>[7–11]</sup> Interestingly, it was possible to switch between the polar configurations by sliding the partial dislocation that separates them, resulting in a phenomena called “interfacial ferroelectricity”.<sup>[10,12,13]</sup> Moreover, distinct multilayer polytypes exhibit

cumulative polarization steps, known as “ladder ferroelectrics”.<sup>[14,15]</sup> This unique opportunity to switch locally between many adjacent diatomic polytypes provides a novel platform to explore their basic quasi-particle response on the one hand, and to exploit their polarization for storage and information processing technologies on the other hand.<sup>[16]</sup>

Polarization in the above-discussed gapped diatomic polytypes emerges from an inherent charge transfer between atoms of different types.<sup>[7]</sup> This is obviously lacking in graphene-layered polytypes – a semi-metallic system of ever-growing interest,<sup>[17–23]</sup> where the constituent layers contain a single atomic species, and are centrosymmetric (as opposed to polar elemental crystals of Tellurium and Bismuth reported recently<sup>[24,25]</sup>). These structures are currently central to a substantial body of experimental and theoretical work, reporting novel effects such as orbital magnetism and unconventional superconductivity in response to external electric fields.<sup>[26–30]</sup> It is therefore interesting to ask whether internal polarization could emerge in this case at all,<sup>[31,32]</sup> and, if so, what would its nature be?

To explore these questions, recall that in a crystal based on one type of atom, unit cell symmetry and nuclear positions within the unit cell determine all crystal properties. Specifically, when graphene is stacked into a bilayer structure, the interface avoids the high-energy fully eclipsed (AA) configuration, adopting instead the optimal (AB) stacking mode, where only half of the

S. S. Atri, B. Alon, N. Roy, M. V. Stern, M. Goldstein, M. Ben Shalom  
 School of Physics and Astronomy  
 Tel Aviv University  
 18, Klausner Street, Tel Aviv 6997801, Israel  
 E-mail: [moshebs@tauex.tau.ac.il](mailto:moshebs@tauex.tau.ac.il)

W. Cao, M. Urbakh, O. Hod  
 Department of Physical Chemistry  
 School of Chemistry  
 The Raymond and Beverly Sackler Faculty of Exact Sciences and The Sackler  
 Center for Computational Molecular and Materials Science  
 Tel Aviv University  
 18, Klausner Street, Tel Aviv 6997801, Israel

V. Falko  
 National Graphene Institute  
 University of Manchester  
 Booth Street East, Manchester M13 9PL, UK

L. Kronik  
 Department of Molecular Chemistry and Materials Science  
 Weizmann Institute of Science  
 234 Herzl Street, Rehovoth 7610001, Israel

 The ORCID identification number(s) for the author(s) of this article can be found under <https://doi.org/10.1002/apxr.202300095>

© 2024 The Authors. Advanced Physics Research published by Wiley-VCH GmbH. This is an open access article under the terms of the [Creative Commons Attribution](https://creativecommons.org/licenses/by/4.0/) License, which permits use, distribution and reproduction in any medium, provided the original work is properly cited.

DOI: 10.1002/apxr.202300095

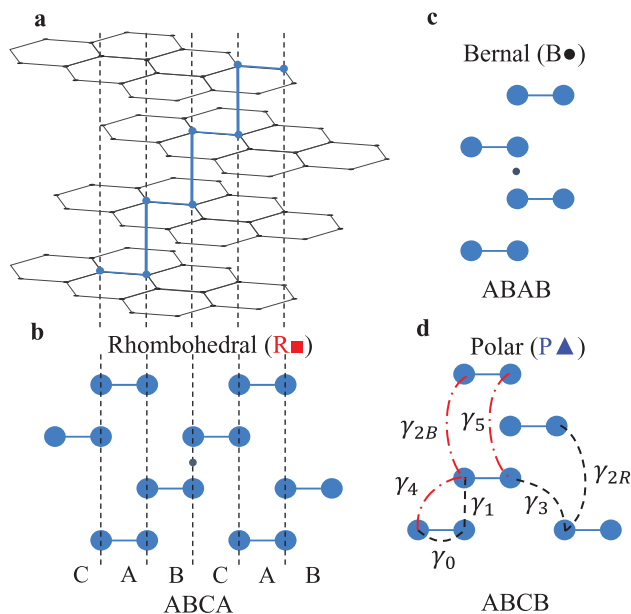


**Figure 1.** Polytypes of four-layered graphene. a) Illustration of the rhombohedral (R, ABCA) polytype, with co-oriented shifts between consecutive layers. b) Cross-section of the R polytype along the in-plane armchair orientation, showing a cyclic shift of carbon pairs between the A/B/C/A positions. c) Cross sectional illustration of the Bernal polytype (B, ABAB) with the inversion center marked by a black circle. d) Cross sectional illustration of the polar polytype (P, ABCB), lacking inversion and mirror symmetries. Various tight-binding model hopping amplitudes are indicated by red dash-dotted and black dashed lines, connecting atoms residing in the same or different sublattices, respectively.

atoms reside atop each other.<sup>[33]</sup> By introducing additional layers, multiple stacking configurations, distinguished by the relative lateral shift between the various layers,<sup>[33–37]</sup> become accessible (see **Figure 1a,b**). For example, in the case of three layers, the crystal can stabilize two high-symmetry polytypes, denoted by ABC or ABA, that preserve inversion [ $x \rightarrow -x$ ,  $y \rightarrow -y$ ,  $z \rightarrow -z$ ] or mirror ( $z \rightarrow -z$ ) symmetry, respectively. In a four-layer stack, the number of polytypes grows to three: (i) the Bernal (B); (ii) the rhombohedral (R) polytypes, both of which break mirror symmetry but preserve inversion symmetry; and (iii) the ABCB (denoted as P) polytype, which breaks both symmetries, allowing for permanent polarization.

Generally, for a stack of an even number  $N$  of layers we find  $2^{N-3} + 2^{(N-4)/2}$  different polytypes possible, all breaking mirror symmetry, out of which only  $2^{(N-2)/2}$  possess inversion symmetry and are hence necessarily non-polar. For an odd number of layers in the stack, we find  $2^{N-3} + 2^{(N-3)/2}$  polytypes, out of which  $2^{(N-3)/2}$  are non-polar centrosymmetric stackings, and  $2^{(N-3)/2}$  are mirror-symmetric configurations that may only present in-plane polarization. The rest of the stacking modes break both symmetries and may exhibit permanent  $P_z$  and in-plane polarization (see detailed discussion in SI.1). For example, for 11 layers ( $N = 11$ ), there are 272 different stacking configurations, out of which 16 are non-polar, 16 may only exhibit in-plane polarization, and 240 may exhibit both out-of-plane and in-plane polarization (see Table S1, Supporting Information).

## 2. Results and Discussion

To explore the possibility of polarization in multi-layered all-carbon graphene stacks, we exfoliate natural graphite flakes on bare silicon oxide ( $\text{SiO}_2$ ) surfaces. We determine the number of graphene layers in each flake from their optical contrast, as well as from their atomic force microscopy (AFM) measured thickness. The marked area in **Figure 2a** shows a typical tetra-layer graphene region with uniform optical and topography maps. However, the integrated Raman map of the same section (**Figure 2b**), constructed by integrating the photon counts in the range  $2674\text{--}2684\text{ cm}^{-1}$  (see **Figure 2c**), reveals three distinct regions, which can be assigned to the above defined B, R, and P polytypes based on their known Raman signatures.<sup>[38]</sup> We further scan the same area by a Kelvin probe force microscope<sup>[39]</sup> to map the room temperature electric surface potential  $V_{\text{KP}}$  (**Figure 2d**). The contrast between polytypes is present also in the electrical measurement, reflecting variations in the work function of the different polytypes.<sup>[23,40,41]</sup> Remarkably, the two P polytype regions that appear with the same color in the Raman map, exhibit different colors in the  $V_{\text{KP}}$  map, clearly demonstrating their opposite internal polarization  $P_{\uparrow}$ ,  $P_{\downarrow}$ . Two line cuts across the polytype regions (solid and dashed black arrows) are presented in **Figure 2e**, demonstrating distinct work function steps between the uniform values corresponding to individual polytypes. To quantify these variations, we consider potential histograms as a function of the number of pixels per potential value, plotted on the right-hand side of **Figure 2e**. Repeating this analysis for many different samples (SI. 3.1) yields  $(V_{\text{KP}}(P_{\uparrow}) - V_{\text{KP}}(P_{\downarrow}))/2 = 6 \pm 1\text{ mV}$ ,  $V_{\text{KP}}(R) - V_{\text{KP}}(B) = 19 \pm 1\text{ mV}$ ,  $V_{\text{KP}}(R) - V_{\text{KP}}(P_{\uparrow}) = 5 \pm 1\text{ mV}$ . These numbers are independent of polytype dimensions, the AFM tool, the environment (ambient versus inert), and the tip type. We note that the average map potential may vary by as much as  $\approx 200\text{ mV}$  in different experiments, yet the potential steps between the polytypes remain unaltered.

The permanent room temperature polarization in a graphitic (seemingly semi-metallic) polytype calls for a careful examination of its doping dependence.<sup>[14,42–44]</sup> To this end, we biased the flakes relative to the bottom Si substrate, thereby forming a planar capacitor that controls the total charge carrier density of the flake<sup>[14]</sup> (**Figure 2a**). We then re-mapped the surface potential for several fixed gate voltages,  $V_g$ , and extracted the potential steps between the different polytypes as a function of the planar charge density  $n$ . As expected, the new maps show  $\pm 10\text{ V}$  variations in  $V_{\text{KP}}$  outside the graphite flakes, corresponding to the applied gate voltage, whereas above the flake  $V_{\text{KP}}$  is altered by merely  $\pm 20\text{ mV}$  (see **Figure S2**, Supporting Information).<sup>[14]</sup> This corresponds to charge accumulation on the flake, with  $n = \pm 2.3 \times 10^{12}\text{ e cm}^{-2}$ , which screens the bottom gate potential (SI 3.2). **Figure 3a** presents the gate and density evolution of the potential step between opposite polar domains  $(V_{\text{KP}}(P_{\uparrow}) - V_{\text{KP}}(P_{\downarrow}))/2$ . Surprisingly, the potential difference and its corresponding internal polarization increase by  $\approx 13\%$  upon hole doping to  $1012\text{ holes cm}^{-2}$ . Such an increase was not observed in layered diatomic structures or in any other system we are aware of, where the added charge distribution typically suppresses the internal polarization.

To rationalize the emergent polarization and explain its unusual dependence on doping, we conducted density functional

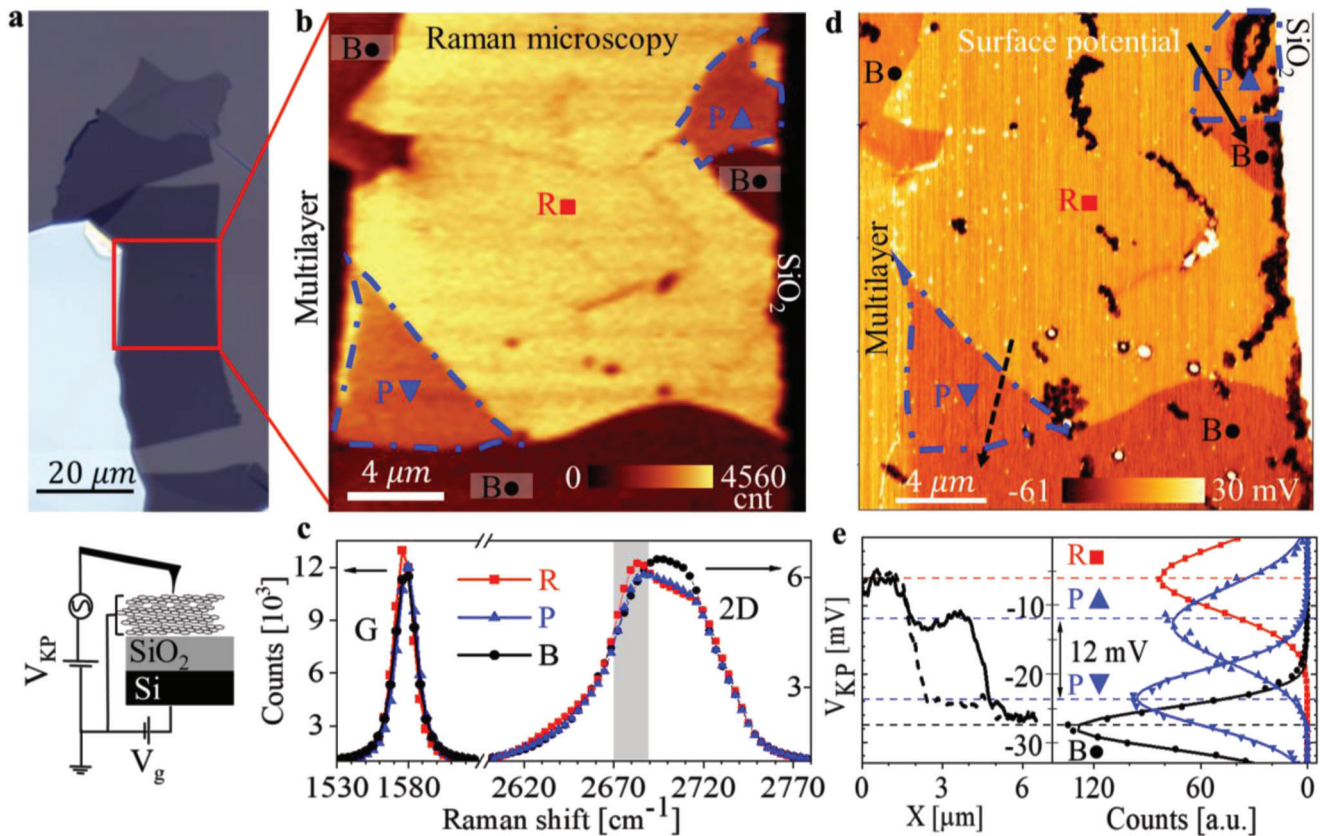


**Figure 2.** Direct observation of internal polarization in graphite. a) Optical image of a typical tetra-layer flake on a Silicon/Silicon dioxide (90 nm) substrate. The cross-sectional illustration at the bottom shows the Gate Voltage ( $V_g$ ) and the Kelvin Probe potential ( $V_{KP}$ ) circuits in the electric force microscopy setup. b) Integrated Raman Intensity map of the area marked in (a) with the color in each pixel representing the number of photons collected at the spectral range, shown as a grey bar in c); The map shows three distinct brightness levels assigned, based on their Raman signatures, to the Rhombohedral (R■), Polar (P▲), and Bernal (B●) polytypes. c) Raman spectra collected from each polytype, showing distinct shifts and intensity variations in the G and the 2D peaks. d) Surface potential map obtained from the same area as in (b); B and R polytypes appear uniform in color and are separated by 17 mV. In contrast, the P polytype appears in two distinct colors. The black areas are typical contamination spots. e) Left: Potential cuts over R-P-B polytypes, along the solid and dashed lines marked in (d); Right: Normalized potential histograms from separate polytype regions and their fitting Gaussians (solid lines).

theory (DFT) calculations (SI. 4.1). The overall  $P_z$  is extracted from the difference between the laterally averaged electrostatic potential far below and above the 2D periodic stack,<sup>[45]</sup> calculated via  $\phi(z) = -\int_{-\infty}^z (z' - z) [\int dx dy \rho(x, y, z')] dz'$ . As expected, the calculated potential is mirror symmetric for the B and R phases, where the polarization vanishes (Fig. 3b, black squares and red dots, respectively). However, for the four-layered P-polytype, a potential difference of  $\approx 6$  mV appears at an electronic temperature of 300K (blue triangles), where the thermal distribution is enforced via appropriate occupation of the Kohn-Sham states. This potential difference is in good agreement with the measured  $(V_{KP}(P_1) - V_{KP}(P_2))/2$  value (Figure 3a). Note the lower potential at the third layer plane of the polar phase (blue curve) versus the B and R phases, indicating a negative charge accumulation in this layer. Figure 3b also shows a cross section of the charge redistribution along the armchair direction after subtracting the charge of the individual layers. The third layer exhibits a pronounced charge difference between the two sublattice sites, while the first and fourth layers show a weaker and opposite response.

Next, we introduce effective doping in the calculation by including fractional nuclear charge “pseudoatoms” that induce excess free charge carriers without violating sample neutrality or distorting the underlying band structure (SI 4.1.2).<sup>[45,46]</sup> The computed doping dependence of the polarization (red curve in Figure 3a) is in overall good agreement with the experiment, showing a slightly larger slope of  $\approx 18\%$  per  $10^{12}$  holes  $\text{cm}^{-2}$ .

The origin of this doping dependence can be rationalized by examining the band structure at the edge of the Brillouin zone near the K point,<sup>[33,35]</sup> where the Fermi level resides (Figure 3c). Unlike the case of the B and R phases (Figure S6, Supporting Information), a gap opening of  $\approx 9$  mV appears between the top of the linear valence band and the bottom of the linear conduction band of the P phase, due to the broken inversion and mirror symmetries. Notably, contributing the most to the density of states (DOS) in the vicinity of the Fermi energy (see Figure 3d) are the flat bands (separated by  $\approx 50$  mV) that are localized on the 1<sup>st</sup> (blue) and 3<sup>rd</sup> (red) layers. These two layers also contribute most to the polarization, with the negative charge on the third layer and the positive one on the first layer. From the projected DOS

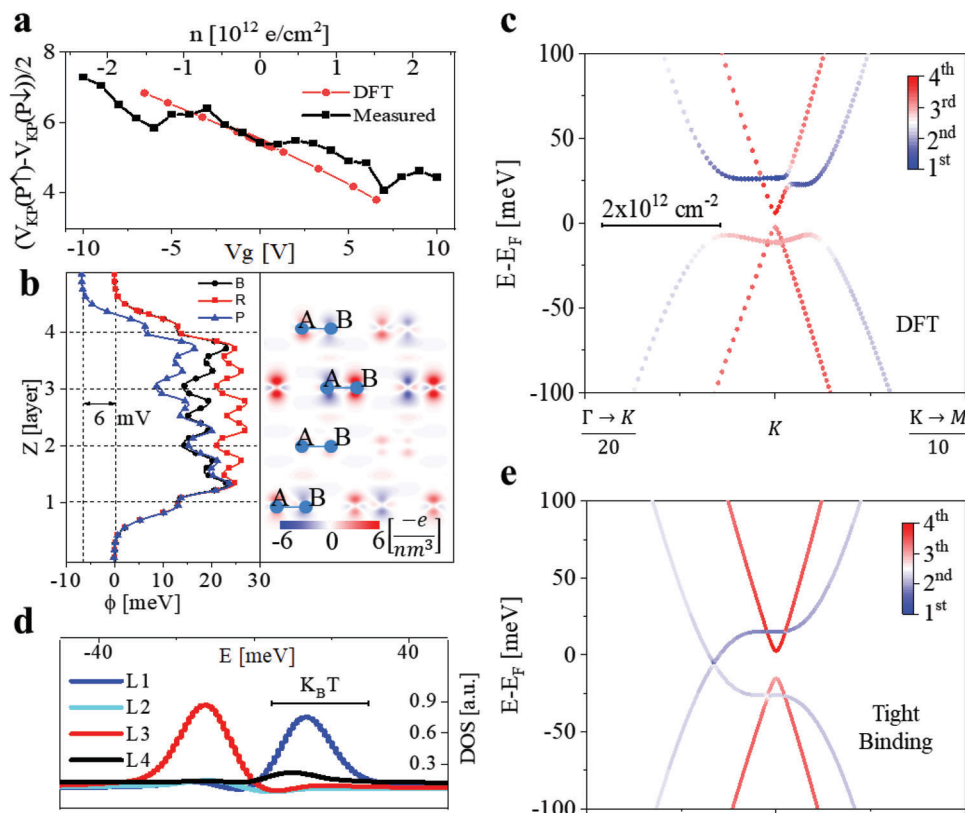


**Figure 3.** Dispersion and doping-dependent polarization of the P tetra-layer polytype. a) The measured (black squares) and calculated (red circles) out-of-plane polarization  $(V_{KP}(P_{\uparrow}) - V_{KP}(P_{\downarrow}))/2$  as a function of the external gate voltage (lower horizontal axis) and the corresponding charge density  $n$  (upper horizontal axis). b) Left: The planar averaged electrostatic potential as a function of the vertical coordinate,  $Z$ , in the three graphitic polytypes. Right: Charge density redistribution map of a cross-section along the armchair direction of the P polytype. Red/blue colors correspond to the residual finite electron/hole density after subtracting the charge distribution of the individual monolayers. c) and e) DFT and self-consistent tight-binding calculated band structures, respectively, centered around the reciprocal K point. The color of the circular symbols marks the wave function projection of the crystal-momentum states on each layer. The scale bar indicates the momentum diameter required to occupy  $2 \times 10^{12}$  cm<sup>-2</sup> states. d) DFT calculated DOS projected on each layer (L1 – L4) as a function of the energy.

(Figure 3d) it becomes evident that as the gate potential becomes more negative, the first and third layers become increasingly depopulated. Because both peaks are within the room-temperature width of the thermal distribution,  $2K_B T \approx 50$  mV, the two layers depopulate by approximately the same charge. However, as the first layer is farther from the center of the tetra-layer stack, its contribution to the polarization dominates and results in an increase of the polarization.

Further insights regarding the microscopic origins of the polarization can be obtained via a tight-binding (TB) model that includes a self-consistent electrostatic potential term. We consider two sites per layer with previously suggested hopping parameters and on-site energies<sup>[47]</sup> (S4.2). The hopping parameters are illustrated in Figure 1d, where we distinguish between coupling of sites on different sublattices (dashed black lines) and on the same sublattice (dash-dotted red lines). An important insight is that if the same-sublattice small amplitudes are neglected, polarization will vanish at charge neutrality due to particle-hole symmetry. Hence our experiment provides a very sensitive probe of them. Still, even when neglecting these terms, polarization would generally become nonzero upon gating. Accounting for these terms, the corresponding polarization will generally decrease with one

sign of the doping, but still increase with the other. This behavior, which is indeed the experimentally observed one, then emerges as typical for graphene polytypes and is inherently different from that observed in polyatomic stacks. The resulting TB band structure is shown in Figure 3e. Several general observations emerge (S4.2): (a) If the self-consistent electrostatic potential is omitted, the calculated polarization disagrees with the experimental and the DFT one in both magnitude and sign.<sup>[31,32]</sup> (b) Allowing for the intra-layer potential differences is crucial for obtaining good agreement with the DFT results; (c) The electron-hole band asymmetry is generally more pronounced in the tight-binding dispersion than in the DFT one.

### 3. Conclusion

We have provided a proof of principle that metastable phases of graphitic stacks can be generated and may exhibit electric polarization. This is explained by DFT calculations as arising from inter-layer charge rearrangement and additionally supported by the fact that self-consistency of the electrostatic potential is essential for the tight binding model. Such 2D Van der Waals polytypes may open venues for constructing and

exploring other elemental yet polar crystals that go beyond the few reported to date in that they rely on inter-layer electronic, rather than intra-layer nuclear, distortions.<sup>[24,25]</sup> We found the room temperature polarization of the graphene multilayer stack to decrease with electron doping, but counterintuitively increase with hole doping. While an increasing polarization with the total charge density has been theoretically suggested,<sup>[48]</sup> to the best of our knowledge this is the first observation of doping-enhanced polarization. We attribute this behavior to gating-induced inter-layer charge transfer, a conclusion supported by the calculated band structure of the non-centrosymmetric stacked system. Despite the semi-metallicity and the non-polar nature of the individual layers the underlying mechanisms pave the way for graphene polarization control by mechanical switching<sup>[28]</sup> or via external gate potentials.<sup>[23]</sup> Specifically, although controllable switching between different graphene polytypes remains an open challenge, we expect novel opportunities for controlling it to arise from small twists between successive layers.

## Supporting Information

Supporting Information is available from the Wiley Online Library or from the author.

## Conflict of Interest

The authors declare no conflict of interest.

## Data Availability Statement

The data that support the findings of this study are available from the corresponding author upon reasonable request.

## Keywords

graphene polytypes, interfacial ferroelectricity

Received: August 30, 2023

Revised: December 31, 2023

Published online:

- [1] A. Guinier, G. B. Bokij, K. Boll-Dornberger, J. M. Cowley, S. Durovic, H. Jagodzinski, P. M. de Wolff, B. B. Zvyagin, D. E. Cox, P. Goodman, T. Hahn, K. Kuchitsu, S. C. Abrahams, *Acta Cryst.* **1984**, *40*, 399.
- [2] Here we use the term polytype in its broad sense,<sup>[1]</sup> which includes metastable 2D arrangements.
- [3] J. Valasek, *Phys. Rev.* **1921**, *17*, 475.
- [4] R. E. Cohen, *Nature* **1992**, *358*, 136.
- [5] P. S. Halasyamani, K. R. Poepfelmeier, *Chem. Mater.* **1998**, *10*, 2753.
- [6] R. Resta, D. Vanderbilt, *Top. Appl. Phys.* **2007**, *105*, 31.
- [7] L. Li, M. Wu, *ACS Nano* **2017**, *11*, 6382.
- [8] Z. Fei, W. Zhao, T. A. Palomaki, B. Sun, M. K. Miller, Z. Zhao, J. Yan, X. Xu, D. H. Cobden, *Nature* **2018**, *560*, 336.
- [9] C. R. Woods, P. Ares, H. Nevison-Andrews, M. J. Holwill, R. Fabregas, F. Guinea, A. K. Geim, K. S. Novoselov, N. R. Walet, L. Fumagalli, *Nat. Commun.* **2021**, *12*, 347.

- [10] M. Vizner Stern, Y. Waschitz, W. Cao, I. Nevo, K. Watanabe, T. Taniguchi, E. Sela, M. Urbakh, O. Hod, M. Ben-Shalom, *Science* **2021**, *372*, 142.
- [11] K. Yasuda, X. Wang, K. Watanabe, T. Taniguchi, P. Jarillo-Herrero, *Science* **2021**, *372*, 1458.
- [12] A. Weston, E. G. Castanon, V. Enaldiev, F. Ferreira, S. Bhattacharjee, S. Xu, H. Corte-León, Z. Wu, N. Clark, A. Summerfield, T. Hashimoto, Y. Gao, W. Wang, M. Hamer, H. Read, L. Fumagalli, A. V. Kretinin, S. J. Haigh, O. Kazakova, A. K. Geim, V. I. Fal'ko, R. Gorbachev, *Nat. Nanotechnol.* **2022**, *17*, 390.
- [13] X. Wang, X. Gao, K. Yang, P. Gu, X. Lu, S. Zhang, Y. Gao, N. Ren, B. Dong, Y. Jiang, K. Watanabe, T. Taniguchi, J. Kang, W. Lou, W. Lou, J. Mao, J. Liu, Y. Ye, Z. Han, K. Chang, J. Zhang, Z. Zhang, *Nat. Nanotechnol.* **2022**, *17*, 1272.
- [14] S. Deb, W. Cao, N. Raab, K. Watanabe, T. Taniguchi, M. Goldstein, L. Kronik, M. Urbakh, O. Hod, M. Ben Shalom, *Nature* **2022**, *612*, 465.
- [15] P. Meng, Y. Wu, R. Bian, E. Pan, B. Dong, X. Zhao, J. Chen, L. Wu, Y. Sun, Q. Fu, Q. Liu, D. Shi, Q. Zhang, Y.-W. Zhang, Z. Liu, F. Liu, *Nat. Commun.* **2022**, *13*, 7.
- [16] M. Lines, A. Glass, Principles and applications of ferroelectrics and related materials **2001**.
- [17] K. S. Novoselov, A. K. Geim, S. V. Morozov, D. Jiang, Y. Zhang, S. V. Dubonos, I. V. Grigorieva, A. A. Firsov, *Science* **2004**, *306*, 666.
- [18] C. H. Lui, Z. Li, Z. Chen, P. V. Klimov, L. E. Brus, T. F. Heinz, *Nano Lett.* **2011**, *11*, 164.
- [19] M. Yankowitz, J. I.-J. Wang, A. G. Birdwell, Y.-A. Chen, K. Watanabe, T. Taniguchi, P. Jacquod, P. San-Jose, P. Jarillo-Herrero, B. J. Leroy, *Nat. Mater.* **2014**, *13*, 786.
- [20] Y. Cao, V. Fatemi, S. Fang, K. Watanabe, T. Taniguchi, E. Kaxiras, P. Jarillo-Herrero, *Nature* **2018**, *556*, 43.
- [21] L. Jiang, S. Wang, Z. Shi, C. Jin, M. I. B. Utama, S. Zhao, Y.-R. Shen, H.-J. Gao, G. Zhang, F. Wang, *Nat. Nanotechnol.* **2018**, *13*, 204.
- [22] J. Yin, S. Slizovskiy, Y. Cao, S. Hu, Y. Yang, I. Lobanova, B. A. Piot, S.-K. Son, S. Ozdemir, T. Taniguchi, K. Watanabe, K. S. Novoselov, F. Guinea, A. K. Geim, V. Fal'ko, A. Mishchenko, *Nat. Phys.* **2019**, *1*, 437.
- [23] H. Li, M. I. B. Utama, S. Wang, W. Zhao, S. Zhao, X. Xiao, Y. Jiang, L. Jiang, T. Taniguchi, K. Watanabe, A. Weber-Bargioni, A. Zettl, F. Wang, *Nano Lett.* **2020**, *20*, 3106.
- [24] G. Rao, H. Fang, T. Zhou, C. Zhao, N. Shang, J. Huang, Y. Liu, X. Du, P. Li, X. Jian, L. Ma, J. Wang, K. Liu, J. Wu, X. Wang, J. Xiong, *Adv. Mater.* **2022**, *34*.
- [25] J. Gou, H. Bai, X. Zhang, Y. Li Huang, S. Duan, A. Ariando, S. A. Yang, L. Chen, Y. Lu, A. T. S. Wee, *Nature* **2023**, *617*, 67.
- [26] Y. Shi, S. Xu, Y. Yang, S. Slizovskiy, S. V. Morozov, S. Son, S. Ozdemir, C. Mullan, J. Barrier, J. Yin, A. Berdiyugin, B. A. Piot, K. Watanabe, T. Taniguchi, V. I. Fal'ko, K. S. Novoselov, A. K. Geim, A. Mishchenko, *Nature* **2020**, *584*, 210.
- [27] H. Zhou, T. Xie, T. Taniguchi, K. Watanabe, A. F. Young, *Nature* **2021**, *598*, 434.
- [28] H. Zhou, T. Xie, A. Ghazaryan, T. Holder, J. R. Ehrets, E. M. Spanton, T. Taniguchi, K. Watanabe, E. Berg, M. Serbyn, A. F. Young, *Nature* **2021**, *598*, 429.
- [29] A. Ghazaryan, T. Holder, E. Berg, M. Serbyn, *Phys. Rev. B* **2023**, *107*, 104502.
- [30] A. Fischer, L. Klebl, J. B. Hauck, A. Rothstein, L. Waldecker, B. Beschoten, T. O. Wehling, D. M. Kennes, Spin and Charge Fluctuation Induced Pairing in ABCB Tetralayer Graphene **2023**.
- [31] A. Garcia-Ruiz, V. Enaldiev, A. Mcellistrim, V. I. Fal'ko, *Nano Lett.* **2023**, *23*, 4120.
- [32] L. Yang, S. Ding, J. Gao, M. Wu, Atypical sliding and Moire ferroelectricity in pure multilayer graphene **2023**.
- [33] M. Aoki, H. Amawashi, *Solid State Commun.* **2007**, *142*, 123.

- [34] F. Guinea, A. H. Castro Neto, N. M. R. Peres, *Phys. Rev. B* **2006**, 73, 245426.
- [35] S. Latil, L. Henrard, *Phys. Rev. Lett.* **2006**, 97, 036803.
- [36] H. Min, A. H. MacDonald, *Prog. Theor. Phys.* **2008**, 176, 227.
- [37] M. Koshino, E. McCann, *Phys. Rev. B – Condens. Matter Mater. Phys.* **2013**, 87, 045420.
- [38] K. G. Wirth, J. B. Hauck, A. Rothstein, H. Kyoseva, D. Siebenkotten, L. Conrads, L. Klebl, A. Fischer, B. Beschoten, C. Stampfer, D. M. Kennes, L. Waldecker, T. Taubner, *ACS Nano* **2022**, 16, 16617.
- [39] W. Melitz, J. Shen, A. C. Kummel, S. Lee, *Surf. Sci. Rep.* **2011**, 66, 1.
- [40] Y.-j. Yu, Y. Zhao, S. Ryu, L. E. Brus, K. S. Kim, P. Kim, *Nano Lett.* **2009**, 9, 3430.
- [41] J. Yu, R. Giridharagopal, Y. Li, K. Xie, J. Li, T. Cao, X. Xu, D. S. Ginger, *Nano Lett.* **2021**, 21, 3280.
- [42] P. Sharma, F.-X. Xiang, D.-F. Shao, D. Zhang, E. Y. Tsybal, A. R. Hamilton, J. Seidel, *Sci. Adv.* **2019**, 5.
- [43] S. C. De La Barrera, Q. Cao, Y. Gao, Y. Gao, V. S. Bheemarasetty, J. Yan, D. G. Mandrus, W. Zhu, D. Xiao, B. M. Hunt, *Nat. Commun.* **2021**, 12, 5298.
- [44] A. Jindal, A. Saha, Z. Li, T. Taniguchi, K. Watanabe, J. C. Hone, T. Birol, R. M. Fernandes, C. R. Dean, A. N. Pasupathy, D. A. Rhodes, *Nature* **2023**, 613, 48.
- [45] A. Natan, L. Kronik, Y. Shapira, *Appl. Surf. Sci.* **2006**, 252, 7608.
- [46] O. Sinai, L. Kronik, *Phys. Rev. B – Condens. Matter Mater. Phys.* **2013**, 87, 235305.
- [47] M. S. Dresselhaus, G. Dresselhaus, *Adv. Phys.* **1981**, 30, 139.
- [48] S. Li, T. Birol, *Phys. Rev. Lett.* **2021**, 127, 087601.